Vortex switching between defects in a magnetic dot

G. M. Wysin*
Department of Physics, Kansas State University, Manhattan, KS 66506-2601

S. Gyan†
Department of Physics, Gettysburg College, Gettysburg, PA 17325
(Dated: October 12, 2008)

A magnetic dot with two defined defects (or holes) is considered as a possible bistable device. For a thin magnet, a single vortex will tend to become pinned on a nonmagnetic defect, and display only in-plane magnetization. With two holes placed symmetrically in a magnetic dot, the single vortex ground state becomes doubly degenerate, due to the two equivalent pinning centers. A Monte Carlo micromagnetics simulation is used to study how an external magnetic field can cause the vortex to switch controllably from one hole to the other. By including inequivalent defined defects, other types of multistable devices could be designed.

PACS numbers: 75.75.+a, 85.70.Ay, 75.10.Hk, 75.40.Mg
Keywords: magnetic vortex, magnetic dot, bistability, defects, Monte Carlo

I. INTRODUCTION: VORTEX IN A DOT WITH DEFECTS

Cylindrical magnetic dots of 1–2 μm diameter and thickness 15–100 nm are of great theoretical and experimental interest, because they could serve as high-density memory devices,[1] using a range of materials including Permalloy,[2,3], Fe[4,5] and Co.[6,7] If a dot is very thin compared to its diameter, demagnetization or dipolar effects lead to a nearly planar magnetization (effective easy-plane anisotropy),[8] that depends on position.[9] At the core of a vortex,[10,11] spins tilt out-of-plane. This effect has been used to identify and locate vortices,[12] which have also been identified using magnetic force microscopy.[13] The core spin tilting is similar to that for vortices in easy-plane magnets,[14–16] whose core spins only tilt out of plane when the anisotropy is weaker than a critical strength,[16,17] which originates from an energetic instability.[18–20] The gross effects of defects in magnetic dots, including dipolar effects, can be gleaned from their effects in 2D easy-plane magnets, including only the effects of anisotropic exchange interactions.

In easy-plane magnets (exchange interactions but no dipolar interactions), theory[21–24] and experiments[25,26] show that nonmagnetic defects attract and pin vortices. Vortex energies are lower on defects[27,28] and defect sites have a thermodynamic preference for vortex formation around their centers.[29] For a vortex pinned on a minimum defect (i.e., one nonmagnetic site in the lattice), all spins obtain a greater tendency to stay close to planar,[27,30] requiring even weaker anisotropy for the core spins to tilt out-of-plane. Considering a hole in the dot as a larger nonmagnetic defect, removing a greater number of magnetic sites beyond some fairly small radius eventually leaves only the planar vortex configuration as the stable one.[31] All these effects still will be present when dipolar forces are included, but to an even greater degree because they increase the effective easy-plane anisotropy. Although the identification of pinned planar vortices may be more difficult in experiments, on the other hand, in some sense the theory is simpler.

The pinning is natural. When formed on a defect, some exchange interactions are removed, compared to a vortex far from a defect, but there is lesser effect on the dipolar energy, leading to the lowered total energy. Pinned vortices in nanoparticles should affect the hysteresis curves[32] and can be manipulated by applied magnetic fields.[12,33] Further, for thin enough dots, there is only weak dependence of magnetization on the (z) coordinate through the thickness. This allows for an approximate two-dimensional analysis.

It makes sense to consider a dot with two intentionally designed defects. The vortex can be attracted by either one, but if the system is symmetrical, then one expects a doubly-degenerate single vortex ground state. We consider simple energetics of these states, and whether an externally applied magnetic field can move the vortex reversibly from one defect to the other, without annihilating it.

We are interested in the finite temperature dynamics of the vortex switching; we apply a Metropolis algorithm Monte Carlo approach. However, for real systems of interest, the computational effort would be too great to follow the dynamics of the atomic spins, because there are too many, in even a 100 nm diameter dot of 15 nm thickness. Instead, the system is partitioned into larger cells containing many atoms, as is done in micromagnetic simulations. There are small errors in this approximation, so it is a way to get an approximate idea of the processes, but without precise estimates of threshold field, etc.

The usual micromagnetics approach uses the Landau-Lifshitz equation with damping to approach to a local minimum energy state. In contrast, we use the Metropolis algorithm to produce a fictitious dynamics, without real time, however, it naturally includes thermal fluctuations which occur in a real system, that could have destabilizing or enhancing effects on the vortex switching process.

Once a vortex is pinned on a defect, there is a threshold applied field needed to free the vortex from the pinning center.[34] Presumably, a field near that strength should be able to move the vortex to an oppositely placed defect in a circular cylinder magnetic dot. Toward that end, we also use a local field relaxation of the magnetic dipoles to show how the presence of holes in a magnetic dot produces an effective potential for vortex motion within the dot.

As a test application, the calculations are carried out for the parameters of Permalloy-79 ($Fe_{21}Ni_{79}$), which has saturation magnetization $M_S = 860$ kA/m, continuum exchange stiffness $A = 13$ pJ/m, Curie temperature near 630 K, and face-centered-cubic lattice structure with conventional unit cell parameter $a_0 = 0.355$ nm.

II. EFFECTIVE ATOMIC HAMILTONIAN

In the underlying atomic system, the spins have atomic magnetic dipole moments of magnitude $\mu_{\rm atom} = g\mu_B S$, where g is the Landee g-factor, μ_B is the Bohr magneton, and S is the spin length. Assuming fcc lattice structure, there are four atoms per conventional unit cell of size a_0^3, giving a volume per atom of $v_1 = a_0^3/4$, and the saturation magnetization is

$$M_S = \frac{g\mu_B S}{v_1}. \tag{1}$$

(With the parameters for Py, this implies atomic dipole moments $\mu_{\rm atom} = 9.62 \times 10^{-24}$ A $\cdot$ m^2.) The spins interact with their nearest neighbors via ferromagnetic exchange of strength J, and with all other spins through long-range dipolar forces. The local anisotropy forces are much weaker, and not included here. The exchange hamiltonian between spins $\vec{S}_i$ on the underlying fcc lattice is

$$H_{\rm ex} = -J \sum_{(i,j)} \vec{S}_i \cdot \vec{S}_j \tag{2}$$

where (i,j) indicates summing over all nearest neighbor pairs with each pair counted once, where i and j denote lattice sites, and J is the atomic exchange constant. J is proportional to the commonly used continuum exchange stiffness A, which is used to define the exchange energy based on the scaled continuum magnetization, $\vec{m} = \vec{M}/M_S$, through

$$H_{\rm ex} = A \int dV \ \nabla\vec{m} \cdot \nabla\vec{m}. \tag{3}$$

These two ways of writing the system exchange exchange energy can be matched, to get the relation bewteen J and A, by making a continuum limit of the discrete hamiltonian (2). Expanding the spins around an arbitrarily chosen central spin on the fcc lattice, and converting the summation to an integration leads to

$$H_{\rm ex} = 2J \int \frac{dV}{a_0^3} \nabla\vec{S} \cdot \nabla\vec{S} \ a_0^2 \tag{4}$$

To arrive at this, a constant energy proportional to the number of spins was dropped. The scaled magnetization $\vec{m}$ is the same as a continuum version of the normalized spin field $\vec{S}/S$, hence it is easy to show the desired relation,

$$JS^2 = \frac{1}{2} A a_0. \tag{5}$$

It may be useful to note that the factor of $\frac{1}{2}$ present here for fcc lattice changes to 2 for simple cubic lattice, and becomes 1 for body centered cubic lattice. In all these cases, a_0 is the size of the conventional cubic cell used to define that lattice. For instance, using $A = 1.3 \times 10^{-11}$ J/m and a lattice constant of 0.355 nm for fcc Permalloy, the relation gives exchange constant $JS^2 = 2.31 \times 10^{-21}$ joules, or $JS^2/k_B = 167$ kelvin, where k_B is Boltzmann's constant.

The dipolar interactions involve the response of one spin to the effective dipolar fields produced by all other spins. Therefore, the dipolar interaction hamiltonian is

$$H_{\rm dd} = -\left(\frac{\mu_0}{4\pi}\right) \sum_{i>j} \frac{[3(\vec{\mu}_i \cdot \hat{r}_{ij})(\vec{\mu}_j \cdot \hat{r}_{ij}) - \vec{\mu}_i \cdot \vec{\mu}_j]}{r_{ij}^3}, \tag{6}$$

where $\hat{r}_{ij}$ is the unit vector pointing from site i towards site j and the $\vec{\mu}_i$ are the atomic dipole moments. The sum with $i > j$ avoids double counting the interactions. In the work here, any demagnetization effects are taken into account via the dipole-dipole interactions. Using the atomic dipoles and distances measured in terms of the lattice parameter of the conventional unit cell, defines the strength of dipolar couplings,

$$D = \left(\frac{\mu_0}{4\pi}\right) \frac{\mu_{\rm atom}^2}{a_0^3}. \tag{7}$$

In Permalloy, this gives $D = 2.07 \times 10^{-25}$ joules, which can be compared with the exchange JS^2 to give an idea of the relative importance of the two energies. We can define the relative dipolar coupling strength δ by their ratio,

$$\delta = \frac{D}{JS^2}. \tag{8}$$

For Py, this fundamental atomic value is $\delta = 8.96 \times 10^{-5}$, which shows that only the combined interactions (or torques) of many dipoles can overcome the local exchange interactions.

Finally an externally generated applied magnetic field, $\vec{B}$, is assumed to act on the spins, with hamiltonian,

$$H_{\rm B} = -\sum_i \vec{B} \cdot \vec{\mu}_i. \tag{9}$$

The system also is assumed to be affected by thermal fluctuations corresponding to the ambient absolute temperature in kelvin, T.

III. MICROMAGNETICS VIEWPOINT

Of course, for typical micron sized dots, the number of individual atoms is too great for computer simulations of such a large number of degrees of freedom. Instead, in the micromagnetic viewpoint, the system is broken up into larger cells, each of which contains many atoms, but which are small enough that the net magnetic moment might have nearly a constant magnitude, but varying direction. The simulations need only keep track of the directions of the magnetic moments in each cell. Obviously it is an approximation. But if the exchange is strong enough, then the spins in a cell stay mostly aligned, hence the dipole moment in a cell has fixed length, equal to the saturation magnetization times the cell volume.

The cells being used do not have to be cubic. In a thin magnet, there is only weak dependence on z, the coordinate measuring distance through the thickness. To a first approximation we can ignore any dependence of $\vec{M}$ on z. Then it makes sense to have cells which are small in xy directions, but long columns in the z direction, and use only a single layer of cells. In this way the problem is converted into an equivalent two-dimensional problem. The working cells can be of dimensions $a\times a\times la$, where a is greater than the atomic lattice parameter a_0, and la is the total thickness of the sample. To be appropriate from the physical point of view, however, la should be small enough, so that the assumption of spins aligned within a cell is still valid. The spins in a cell being aligned means the magnetization is assumed to be saturated in each cell. The cell edges are assumed to be much smaller in the xy directions, where the magnetization changes more rapidly with position.

The volume of a working cell being $v_{\rm cell} = la^3$, contains many atoms. Assuming the atoms fill an fcc lattice as for Permalloy, the number of atoms in a working cell must be $la^3/(a_0^3/4)$. Then the saturated magnetic moment $\mu_{\rm cell}$ in a cell would be

$$\mu_{\rm cell} = M_s v_{\rm cell} = \frac{g\mu_B S}{a_0^3/4}\times la^3 = 4l\left(\frac{a}{a_0}\right)^3 \mu_{\rm atom}. \quad (10)$$

For most of the studies here, we consider a Permalloy disk 10 nm thick, and use a cell size $a = 1.5$ nm. This results in $\mu_{\rm cell} = 2010\ \mu_{\rm atom}$. In the micromagnetics viewpoint, these will be taken as the fixed magnitude dipoles that interact with each other via local exchange and long-range dipolar forces. They only need to be defined on a two-dimensional grid, but we need to know their effective couplings that would enter the Monte Carlo scheme.

A. Exchange interactions

For the exchange interactions, we use the general expression (3) converted to a finite difference representation on the chosen cell grid. Although the underlying atomic interactions live on the fcc lattice, those interactions are thought of as smoothed out, and now we just have the cell-to-cell exchange interactions. We assume a square cell grid (ignoring the z-dependence). A cell centered at the origin is surrounded by four other cells, at displacements of $\pm a\hat{x}$ and $\pm a\hat{y}$ (measured to their centers). Then the exchange energy of our cell at the origin interacting with only the two neighbors to the right and above, as a lowest order finite difference approximation to (3), is

$$H_{\rm ex,cell} = Av_{\rm cell}\times \left\{\left(\frac{\vec{m}(a\hat{x})-\vec{m}(0)}{a}\right)^2 + \left(\frac{\vec{m}(a\hat{y})-\vec{m}(0)}{a}\right)^2\right\}. \quad (11)$$

We use only these two neighbors; then by summing over all cells, there will be no double counting, as every cell-to-cell bond will be included only once. Expanding and re-arranging, this becomes

$$H_{\rm ex,cell} = \frac{Av_{\rm cell}}{a^2}\left\{4\vec{m}^2 - 2\vec{m}(0)\cdot[\vec{m}(a\hat{x})+\vec{m}(a\hat{y})]\right\}. \quad (12)$$

But the magnetization vectors $\vec{M}$ that produce $\vec{m} = \vec{M}/M_S$ in each cell have been assumed to be saturated to the value M_S. It means that the each $\vec{m}$ is a unit vector, so the per-cell exchange contribution is

$$H_{\rm ex,cell} = \frac{2Av_{\rm cell}}{a^2}\left\{2 - \vec{m}(0)\cdot[\vec{m}(a\hat{x})+\vec{m}(a\hat{y})]\right\}. \quad (13)$$

Finally, it can be expressed as the exchange energy per bond,

$$H_{\rm ex,bond} = \frac{2Av_{\rm cell}}{a^2}\left[1 - \vec{m}(0)\cdot\vec{m}(a\hat{x})\right]. \quad (14)$$

It demonstrates that the effective exchange coupling between the cells (i.e., cell-to-cell) is

$$J_{\rm cell} = \frac{2Av_{\rm cell}}{a^2} = \frac{2A(la^3)}{a^2} = 2Aal = 2lAa_0\left(\frac{a}{a_0}\right). \quad (15)$$

By using the connection (5) from A to the atomic exchange coupling on the fcc lattice, we get

$$J_{\rm cell} = 2l(2JS^2)\frac{a}{a_0} = \frac{4la}{a_0}JS^2. \quad (16)$$

This will be needed to execute the micromagnetics for our choice of cell size, inputted by parameters l and a/a_0, based on the atomic exchange coupling of the fcc lattice. It is interesting that it depends on $4\times$ the height of the micromagnetics cell, la, compared to the conventional cell edge of the fcc lattice, a_0. For simulations here with cell size $a = 1.5$ nm, and dot thickness $la = 10$ nm, the relation gives $J_{\rm cell} = 113\ JS^2$.

B. Dipolar interactions

The exchange strength between cells can be contrasted to the strength of their effective dipolar interactions. We

already saw that each cell has a dipole moment of magnitude $\mu_{\rm cell} = (4la^3/a_0^3)\mu_{\rm atom}$. These interact as well according to a Hamiltonian like Eq. (6), but substituting the atomic dipoles with these cell dipoles. Also, lengths (or positions) will be measured in units of the cell size, a, and it is convenient to use the unit vector magnetic moments (fictitious "spins"), $\hat{\sigma}_i = \vec{\mu}_i/\mu$. Thus we have the dipolar terms convenient for micromagnetics calculations,

$$H_{\rm dd} = -\frac{\mu_0}{4\pi}\frac{\mu_{\rm cell}^2}{a^3}\sum_{i>j}\frac{[3(\hat{\sigma}_i\cdot\hat{r}_{ij})(\hat{\sigma}_j\cdot\hat{r}_{ij}) - \hat{\sigma}_i\cdot\hat{\sigma}_j]}{(r_{ij}/a)^3}. \quad (17)$$

This leads us to define the effective dipolar coupling strength, using the cell's magnetic moment and size,

$$D_{\rm cell} = \left(\frac{\mu_0}{4\pi}\right)\frac{\mu_{\rm cell}^2}{a^3}. \quad (18)$$

Substituting the cell's magnetic moment, it is interesting to quote this in units of the atomic dipolar coupling, viz.,

$$D_{\rm cell} = \left(\frac{\mu_0}{4\pi}\right)\frac{[(4la^3/a_0^3)\mu_{\rm atom}]^2}{a^3} = \frac{16l^2a^3}{a_0^3}\times D, \quad (19)$$

where the atomic dipolar coupling strength D is defined in Eq. (7). D gets enhanced for a cell by the factor $(4l)^2(a/a_0)^3$. Taking the cell-to-cell exchange as the basic energy unit, the dipole to exchange ratio is

$$\delta_{\rm cell} \equiv \frac{D_{\rm cell}}{J_{\rm cell}} = \frac{D(4l)^2(\frac{a}{a_0})^3}{4l\frac{a}{a_0}JS^2} = \left[\frac{D}{JS^2}\right]\times 4l\left(\frac{a}{a_0}\right)^2, \quad (20)$$

which will indicate the relative dipole coupling strength in the micromagnetics. Of course, the quantity $\delta = D/JS^2$ just represents the corresponding strength of dipolar couplings to exchange couplings in the atomic system. For Permalloy with $\mu_{\rm atom} = 9.62\times10^{-24}$ A·m^2, the atomic values $D = 2.07\times10^{-25}$ joules and $JS^2 = 2.31\times10^{-21}$ joules give the fundamental value $\delta = 8.96\times10^{-5}$. So the net enhancement of that, for the interactions of the micromagnetics cells, is by the factor $4l(a/a_0)^2$.

$$\delta_{\rm cell} = \delta\times 4l\left(\frac{a}{a_0}\right)^2. \quad (21)$$

We used simulations with $la = 10$ nm and $a = 1.5$ nm, which gives $\delta_{\rm cell} = 476\ \delta = 0.0427$, a moderate value for the relative dipolar strength, rather than an excessively strong or weak value that could slow down the calculations or produce numerical artifacts.

C. Energy, temperature and magnetic field considerations

Exchange and dipole terms form the intrinsic or internal system energy,

$$H_{\rm int} = H_{\rm ex} + H_{\rm dd}. \quad (22)$$

One of the primary interests will be in the evolution of $H_{\rm int}$ over any barrier during a switching process.

It is usual in the Monte Carlo to express all energies (and the temperature) in units of the exchange constant. But in the micromagnetics, the exchange coupling is enhanced for the cells, compared to the underlying atomic exchange couplings. We need to consider how this affects the definition of the temperature being used. Also related is to get the appropriate dimensionless unit for applied magnetic field.

The system is exposed to an externally generated magnetic field (i.e., magnetic induction $\vec{B}$), which provides an additional energy term,

$$H_{\rm B} = -\sum_{\rm atoms\ i} g\mu_B\vec{S}_i\cdot\vec{B} \to -\sum_{\rm cells\ i}\vec{\mu}_i\cdot\vec{B}. \quad (23)$$

It is important to note that $\vec{B}$ is really just the external field, and does not include any demagnetization field, because that effect is actually included in the dipolar interactions, which produce fields that act between the dipoles. By scaling out a factor of $J_{\rm cell}$ from the magnetic hamiltonian, and using the cell dipole, $\mu_{\rm cell} = (4la^3/a_0^3)\mu_{\rm atom}$, we get the rescaled magnetic part, in terms of the unit magnitude dipoles in the cells (each $\vec{\mu}_i = \mu_{\rm cell}\,\hat{\sigma}_i$),

$$H_{\rm B} = J_{\rm cell}\ \vec{b}\cdot\sum_i\hat{\sigma}_i, \quad (24)$$

where the dimensionless field is

$$\vec{b} = \frac{\mu_{\rm cell}\vec{B}}{J_{\rm cell}} = \frac{4l\frac{a^3}{a_0^3}\mu_{\rm atom}\vec{B}}{4l\frac{a}{a_0}JS^2} = \left(\frac{\mu_{\rm atom}}{JS^2}\right)\left(\frac{a}{a_0}\right)^2\vec{B}. \quad (25)$$

For permalloy, the atomic factor is

$$\frac{\mu_{\rm atom}}{JS^2} = \frac{9.62\times10^{-24}\ {\rm A\cdot m^2}}{2.31\times10^{-21}\ {\rm joules}} = 0.00416\ {\rm tesla}^{-1}. \quad (26)$$

Using the cell size $a = 1.5$ nm with conventional unit cell $a_0 = 0.355$ nm, then

$$\left(\frac{\mu_{\rm atom}}{JS^2}\right)\left(\frac{a}{a_0}\right)^2 = (0.00416\ {\rm T}^{-1})\times\left(\frac{a}{a_0}\right)^2 = 0.0743\ {\rm T}^{-1}. \quad (27)$$

Of course this would give the conversion into dimensionless field,

$$\vec{b} = (0.0743\ {\rm T}^{-1})\times\vec{B}. \quad (28)$$

A typical dimensionless field as small as $b = 0.05$ then corresponds to a fairly strong laboratory field strength, $B = 0.67$ T.

The total hamiltonian includes applied field, exchange, and dipolar forces. When an overall factor of $J_{\rm cell}$ is taken out of the total hamiltonian, we get the effective

micromagnetics hamiltonian involving the "spins" $\hat{\sigma}_i$ in the working cells,

$$H = J_{\rm cell}\left\{\sum_{(i,j)}\hat{\sigma}_i\cdot\hat{\sigma}_j - \sum_i \vec{b}\cdot\hat{\sigma}_i + \delta_{\rm cell}\sum_{i>j}\frac{[3(\hat{\sigma}_i\cdot\hat{r}_{ij})(\hat{\sigma}_j\cdot\hat{r}_{ij})-\hat{\sigma}_i\cdot\hat{\sigma}_j]}{(r_{ij}/a)^3}\right\}. \quad (29)$$

In the simulation programs, the dimensionless parameters $\delta_{\rm cell}$ and $\vec{b}$ are provided as inputs, with the assumption that all energies are measured in units of $J_{\rm cell}$, and distances are measured in units of cell size a.

The last energy issue is the effective temperature for the micromagnetics. But every energy quantity is being measured in units of $J_{\rm cell}$. So the Monte Carlo simulations take as input the Boltzmann energy k_BT in the same units, via the dimensionless temperature τ defined by

$$\tau = \frac{k_BT}{J_{\rm cell}} = \frac{k_BT}{4l\frac{a}{a_0}JS^2}. \quad (30)$$

For permalloy, we saw $JS^2/k_B = 167$ kelvin. Then, the 10 nm thick system has $la = 10$ nm, and using $a_0 = 0.355$ nm, leads to the conversion,

$$\tau = \frac{T\times 0.355\ \text{nm}}{4\times 10\ \text{nm}\times 167\ \text{kelvin}} = \frac{T}{18820\ \text{K}}. \quad (31)$$

This result means that even for modelling the system at room temperature of 300 K, the dimensionless temperature will be only $\tau \approx 0.0159$, so low that Monte Carlo may not work very well. For completeness, it is good to realize a different form for τ:

$$\tau = \frac{k_BT}{\frac{4la}{a_0}\times\frac{1}{2}Aa_0} = \frac{k_BT}{2\ la\ A}. \quad (32)$$

It shows the simple inverse relationship between the system thickness la and the reduced temperature–but there is no adjustment possible for exchange stiffness A. Based on this, the effective temperature τ is reduced dramatically for the cells compared to the underlying atomic spins. The only way to get a larger effective temperature: use many layers in the z-direction (each with effectively $l = 1$), really incorporating the dependence of magnetization on the vertical coordinate through the magnet.

It is important to keep the limits of this thermal micormagnetics in mind. An individual cell has had all its many spin degrees of freedom reduced: most are now internal to the cell, corresponding to slight motions that can make larger changes in exchange and dipolar energies in the cell, but invisible in the micromagnetics. The only visible degrees of freedom left are those corresponding to the orientation of the total cell dipole $\hat{\sigma}_i$, just two degrees of freedom. Clearly it is an approximation, but better at low temperature, where exchange dominates and keeps neighboring spins close to perfect alignment. These results explain why micromagnetics can work well: the effects of temperature are secondary to such an extent that they can almost be ignored, as long as the fundamental micromagnetic assumptions hold (nearly saturated magnetization within cells, due to the dominance of exchange interactions). However, the multitude of atomic spin motions within a cell have been replaced by just one magnetic dipole, so short length scale magnetization variations may not be correctly represented. It is important to remain aware that the detailed structure of vortices, especially near their core, will not be correctly described.

D. Monte Carlo micromagnetics approach

We use a spin Monte Carlo simulation[35,36] to make the system evolve, as an alternative to the usual application of the Landau-Lifshitz-Gilbert equation with damping. In this way, evolution over an energy barrier can take place due to thermal fluctuations.

The dipolar interaction energy is computationally intensive, because all N cells interact with every other cell, making $N(N-1)/2$ total dipolar terms in Eq. (17). When one cell is changed, all the dipole interaction terms can change. Due to the long-range dipolar couplings, a cluster approach is not possible. One way to improve speed on larger systems is to incorporate a fast Fourier transform to reciprocal space[37], at the expense of more complex programming. Using that type of MC scheme, Sasaki and Matsubara[37] showed the transition from quasi-single domain state to vortex state with increasing dot size. Here we apply only a simple local update scheme, based on the Metropolis algorithm, as has been applied in various spin models.[38–40] One Monte Carlo sweep (MCS) is defined as making one trial change on every cell, selected at random in the system. Having selected a cell, a small random trial change is applied to its moment $\hat{\sigma}_i$, by adding a vector increment of fixed length but random direction, followed by rescaling to unit length. The possible energy change ΔE is then calculated, using hamiltonian (29). If $\Delta E \le 0$, the change is accepted, but if $\Delta E > 0$, the change is accepted only with the probability given by the Boltzmann factor, $p = \exp(-\beta\Delta E)$, where $\beta = \tau^{-1}$. (Of course, all energies are evaluated in units of $J_{\rm cell}$ as discussed earlier.) The spin increments are dynamically changed during the MC to maintain the acceptance rate of moves between 30% and 60%. Repeated calculations of inter-cell distances and their powers were avoided by storing these numbers in arrays to speed up the dipole energy evaluation.

IV. TWO DEFECT SYSTEM AND VORTEX SWITCHING

A single vortex in a circular magnet with two well separated defects or holes should be stable on either hole,

especially if the holes are located symmetrically in the system. This system can be a prototype for studying a switching between two equivalent states of the vortex. We are mainly interested in two aspects of this problem. The first is to quantify the ability of one of the holes to attract and pin the vortex, with no applied field, and the second is to evaluate the applied magnetic field strength needed to cause a vortex pinned on one hole to be moved to the other hole. Of course, with two holes present, there should be an effective potential felt by the vortex, that describes the competition between the two holes to grab the vortex. It would be instructive to see the form of this potential, and get estimates of the depth of the attractive parts on the holes, as well as the size of the peak or saddle between the holes. A complete description would show how the potential changes with the applied field, which must cause the potential well of one hole to become deeper, while the other hole's potential well becomes shallower.

It is known than a minimum applied field is needed even to de-pin a vortex from a defect.[34] Thus, we need to know what field strength will succeed to free the vortex from one hole and then transfer it in a controlled and stable manner to the other hole. The answer must depend at least partially on the arrangement of the holes, their size compared to the dot size, the material parameters, the temperature, and so on. Other issues to be addressed would involve the stability of the switching process. If the applied field is too strong, instead of switching the vortex, it may simply annihilate the vortex or remove it from the dot.

To describe the switching process means to initiate the MC simulations with a vortex on one hole, or perhaps away from both holes, and then running the MC while monitoring the vortex motion and other characteristics. It makes sense to base the description on that for vortices in a pure circular magnetic dot, without defects. In general, the spins (or the cell dipoles) can be described by their in-plane angles Φ_i and a corresponding out-of-plane component, σ_i^z. For a defect-free dot of adequate size, the vortex ground state can be described by giving the in-plane angles as

$$\Phi_i = \phi_i + \phi_0, \tag{33}$$

where $\phi_i = \tan^{-1}(y_i/x_i)$ is the azimuthal coordinate measured with respect to the dot center, and $\phi_0 = 90°$ is a constant global rotation of all the dipoles away from the radial direction.

The vortex would actually have two equivalent states at $\phi_0 = \pm 90°$, corresponding to opposite directions of the circulation of the spins around the center of the dot (circulation $C = +1$ for $\phi_0 = +90°$ and $C = -1$ for $\phi_0 = -90°$). The switching of that degree of freedom of the vortex, could be caused by an applied field,[41] or by a current through the dot.[42] The out-of-plane component σ_z is monotonically decreasing outward from the vortex core. An approximate analytic expressions has been given (rigid vortex model)[43] and its switching (of the vortex "polarization") has also been of considerable interest.[44,45] For our work here, however, when a vortex is pinned into a hole, even an extremely small hole will cause the spins to remain essentially lying within the xy-plane, the plane of the dot, so we assume $\sigma_z = 0$ and there is no polarization. Therefore, we can initiate a planar vortex into the system by using expression (33), but centered on one of the holes. It may not be exactly the correct form, however, some initial equilibration MC steps are taken (1000 to 2000 MCS) to allow the spins to relax to accomodate the corrections caused by the system geometry and the dipolar forces, before turning on any external magnetic field.

During the simulation, the vortex core location can be defined roughly as within the cell where the effective vorticity charge is found, i.e., where the following integral around the cell edges gives $q = 1$:

$$q = \frac{1}{2\pi} \oint \vec{\nabla}\Phi \cdot d\vec{r}. \tag{34}$$

Another indication of the motion of the vortex between the holes, and the associated changes in the spin field, can be obtained by defining a kind of *relative circulation* or relative curling, with respect to each hole as a center:

$$C_{\rm hole} = \frac{1}{N} \sum_i \hat{\sigma}_i \cdot \hat{\phi}_{\rm i,\ hole}. \tag{35}$$

The subscript "hole" is meant to indicate that the azimuthal unit vector at cell i is defined using one of the holes as the origin, rather than with respect to the center of the magnetic dot. There will be a circulation defined this way for each hole. The relative circulation around a hole includes the effects of the thermal fluctuations, as the spins do not always point exactly along the local azimuthal directions around a hole. Thus, each $C_{\rm hole}$ will be less than 1.0 in magnitude. The vortex switching from one hole to the other can be indicated when one circulation falls while the other one rises. If both circulations fall together, then it may indicate that annihilation of the vortex is taking place.

The two equivalent states of the vortex, pinned on either hole, must be separated by an energy barrier if the states are stable. Therefore, the other important quantity to be monitored during the switching is the internal energy $H_{\rm int}$, which includes the exchange and dipolar energies. It is apparent that this energy barrier should have a contribution that increases linearly with the dipolar coupling strength for the atomic spins D [see Eq. (17)]. The role of the exchange is less obvious, however, one aspect is clear. The discreteness of the lattice leads to a certain minimum input energy (or applied field), due to exchange, just to pull the vortex out of the hole. This may not be correctly estimated in the micromagnetics, due to the cell discretization being considerably stronger than the underlying atomic discreteness. It is a difficulty of trying to describe a highly singular structure such as a vortex on a coarse grid, which introduces severe errors near the vortex core. Of course, once the vortex

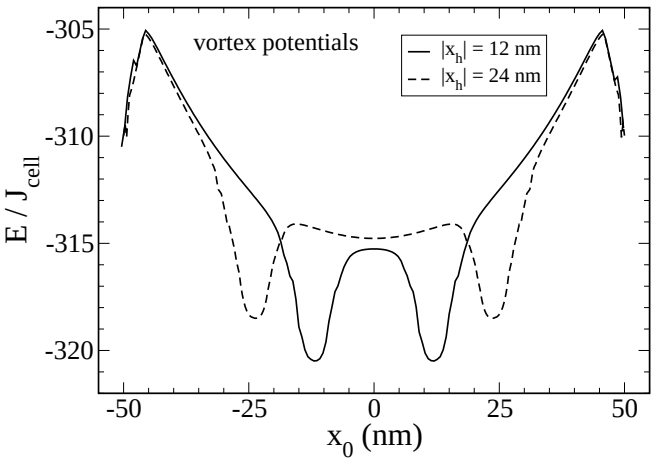

FIG. 1: The effective vortex potential (by zero-temperature local relaxation), for a dot with two holes of 6.0 nm diameter symmetrically located 12 nm from the dot center (solid curve) or 24 nm from the dot center (dashed curve). The dot diameter is 100 nm, thickness 10 nm, with relative dipolar coupling of $\delta_{\rm cell} = 0.0427$, for cell size $a = 1.5$ nm. The curves show the system energy $E(x_0)$, where $\vec{X} = (x_0, 0)$ is the vortex location.

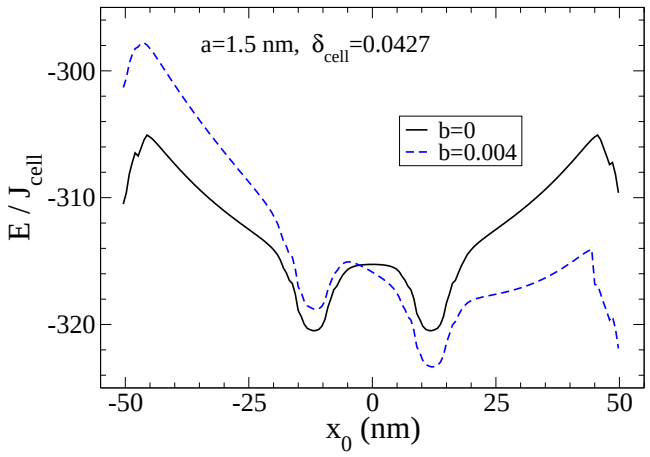

FIG. 2: An example of how the effective vortex-in-dot potential changes with applied magnetic field b perpendicular to the line connecting the holes, for a magnetic dot of 10 nm thickness, diameter 100 nm, and 6 nm diameter holes located 12 nm from the center. For these parameters and Permalloy, $b = 0.004$ corresponds to a field strength $B = 54$ mT.

has moved away from either hole, the dipolar energetics should dominate in determining the net energy barrier.

A. Micromagnetics numerical parameters

The simulations were performed for a 100 nm diameter disk of Permalloy 10 nm thick, somewhat smaller than many of the samples used in experiments. We used a cell size of $a = 1.5$ nm, lattice constant $a_0 = 0.355$ nm, disk thickness $la = 10$ nm, exchange stiffness $A = 13$ pJ/m, and temperature 300 K. As described above, these lead to dimensionless simulation parameters $\delta_{\rm cell} = 0.0427$, and a reduction to effective temperature $\tau = 0.0159$ (in units of $J_{\rm cell} = 2Aal = 2.6 \times 10^{-19}$ joules, or $J_{\rm cell}/k_B = 18820$K). The defects were taken as holes of 6.0 nm diameter. With these parameters, there are about $\pi \times (50./1.5)^2 \approx 3500$ cells needed, which is computationally tractable via Monte Carlo simulation. Alternatively, some additional simulations were carried out using cells with $a = 2.0$ nm for faster execution.

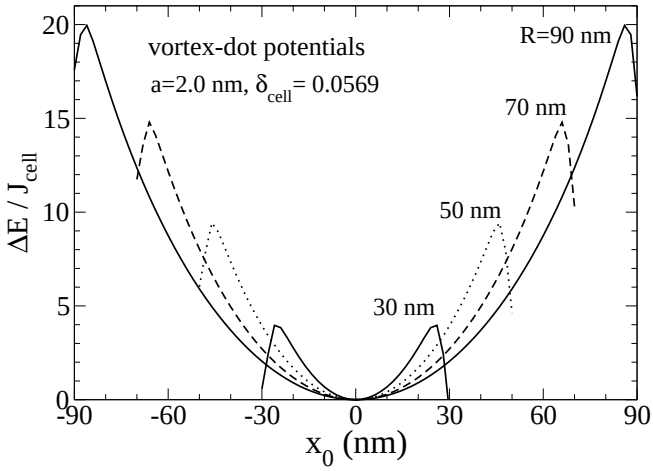

FIG. 3: The effective overall vortex-in-dot potential in magnetic dots of 10 nm thickness with different radii R, without holes. The method is the same as for Fig. 1, but a larger cell size was used to access larger dots. For each curve, the energy has been shifted by the vortex energy when centered in the dot, to give $\Delta E = E(x_0) - E(0)$.

B. Effective Vortex-Hole Potential

The approximate shape of the potential experienced by a vortex can be obtained through a zero-temperature calculation of the total system energy for a sequence of constrained vortex locations, $\vec{X} = (x_0, y_0)$. Simple energy minimization of an initial configuration with a vortex, however, is inadequate. It would lead to a motion of the vortex away from its initial location, quite likely, into one of the holes or out of the system. Instead, an energy minimization must be carried out while artificially "holding" the vortex in place at position $\vec{X}$. This can be done by using a constraining procedure like that in Ref. 46. The energy minimization is carried out while fixing the in-plane angles Φ_i of six "core" dipoles that are nearest to the desired vortex position, at the planar vortex values given similar to Eq. (33),

$$\Phi_i = \tan^{-1}\left(\frac{y_i - y_0}{x_i - x_0}\right) + \phi_0. \qquad (36)$$

(Six core sites were chosen instead of four to try to avoid undesired vortex-antivortex pair configurations.) The global constant is set to $\phi_0 = 90°$ to minimize the dipolar energy. This constraint is applied only to the in-plane components of the six core sites; all other sites and *all* z-components are allowed to change freely. The definition of core sites is rather liberal. If the vortex position $\vec{X}$ is somewhere inside a hole, then the six cells whose centers fall closest to $\vec{X}$ are considered the core, although they fall along the edge of the hole, and might be well-separated from $\vec{X}$ and from each other.

For each chosen vortex position $\vec{X}$, the energy is minimized by an iterative "local field" relaxation.[46] A cell is selected randomly, and then its dipole is redirected to point along the effective magnetic field $\vec{B}_i^{\rm eff}$, produced by exchange with its neighbors and the dipolar forces due to all other sites, and the external field. That is, the total hamiltonian (29) can be expressed in a form, $H = -\sum_i \vec{\mu}_i \cdot \vec{B}_i^{\rm eff}$, which gives an implicit definition of the effective field. One iteration step involves changing N cells. Then typically it requires hundreds or even thousands of iterations until the energy becomes accurate to 1 part in 10^7. The iteration was stopped when the average changes in the unit vector spin components fell below 10^{-7}, according to $\langle|\sigma_x| + |\sigma_y| + |\sigma_z|\rangle < 10^{-7}$. The whole procedure is approximate, due to the constrained cells, but we only want to get a rough idea of the forces and effective potential to which the vortex is exposed.

Fig. 1 shows the resulting potential after the completed relaxation scheme, for the parameters to be used in the MC studies (based on cell size $a = 1.5$ nm), with the holes placed symmetrically in the dot. The vortex position $\vec{X} = (x_0, y_0)$ is scanned from one end of the dot to the other, on the line passing through the holes ($y_0 = 0$). Although it may be somewhat artificial to specify the vortex location inside a hole, the procedure gives a reasonable view of the depth of potential that a hole causes. There is plateau with slight upward curvature in the potential between well-separated holes. Further calculations also show that the depth of the hole potentials increases for larger holes. These results show how stable vortex switching should be better enabled when the holes are not placed too close to the dot's edges. By keeping the holes closer to the dot center, there is a higher potential for the vortex in the region between a hole and the dot's edge, leading to a greater chance of keeping a switched vortex within the dot.

It is interesting to see how the potential changes when a small applied field ($b = 0.004$ or $B = 54$ mT) is turned on, in a direction that tends to make one hole an energetically prefered position compared to the other hole, see Fig. 2. The applied field has a polarizing effect on the vortex structure, which substantially modifies the effective potential, causing a potential energy contribution approximately proportional to x_0. One hole's potential well becomes shallower while the other's becomes deeper. It is clear there will be a minimum field strength to pull the vortex out of the potential well of one hole. As long as the field is strong enough but not too strong, it should be able to pull the vortex out of the first hole, and transfer it to the second in a stable fashion. But this will work only if there is a high enough relative potential near the dot's edge, thus it is important to see how that changes with the dot size. Fig. 3 shows vortex-dot potential for different sized dots not containing holes, showing how the depth of the overall potential well increases with dot size. Our simulations are somewhat limited to smaller dot sizes, however, the switching of a vortex from one hole to another (without being swept out of the dot) should become more managable in a larger dot, due to its deeper overall potential, compared to the potential wells of the holes.

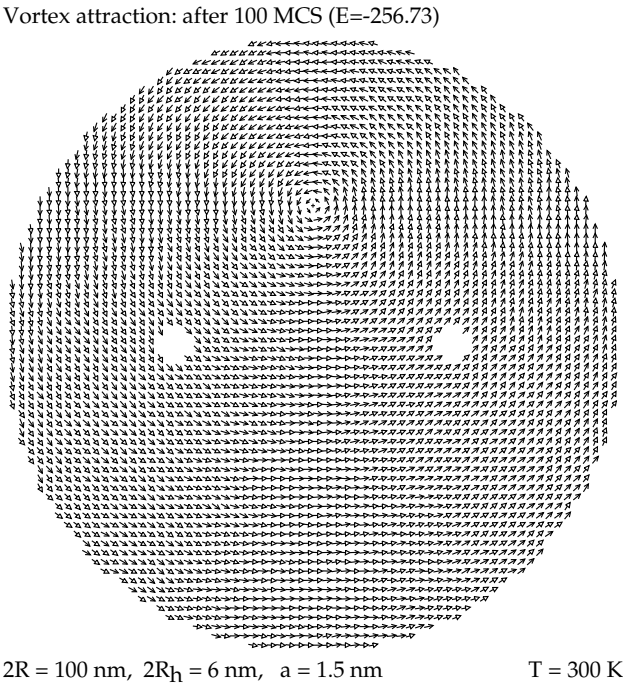

FIG. 4: A starting vortex (at 100 MCS) equidistant from both holes (at $x = \pm 22.5$ nm), for dot diameter of 100 nm, thickness 10 nm, relative dipolar coupling $\delta_{\rm cell} = 0.0427$, with no applied field. Shown is the in-plane projection of the magnetic configuration. The energy is in units of $J_{\rm cell}$. It is allowed to relax via MC at $T = 300$ K.

C. Vortex attraction to a hole

A Monte Carlo simulation is used to confirm the actual attraction caused by 6.0 nm diameter holes, by initiating a planar vortex symmetrically away from but equidistant from two holes centered 22.5 nm ($15a$) from the dot center. After a small number of MC steps, the vortex develops out-of-plane spin components (Fig. 4), which help it to be pulled dynamically towards one of the holes. The initial attraction toward either hole should be equivalent.

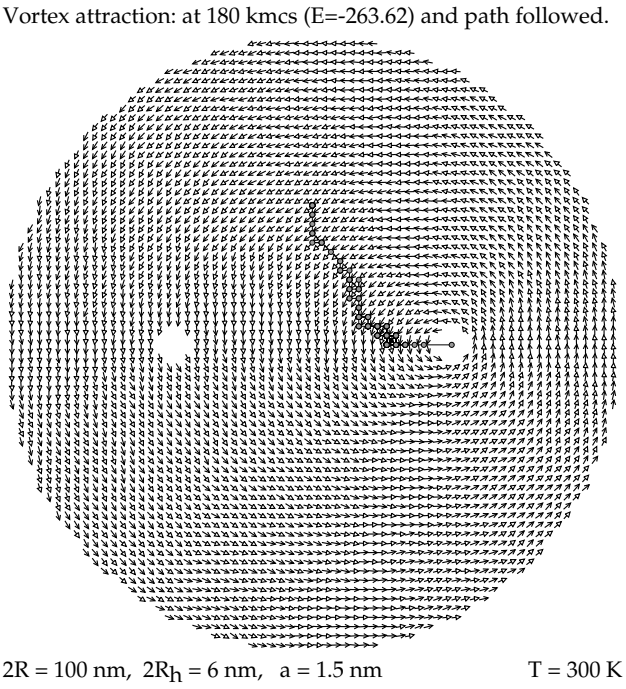

FIG. 5: End of the simulation shown in Fig. 4. The vortex finally gets pinned on the right hole and stays there, in planar form, around 180 kMCS. The magnetic energy has reduced by $6.9J_{\rm cell}$ due to the pinning, compared to its starting location of Fig. 4, giving a sense of the depth of the effective potential.

Due to the randomness of the Monte Carlo, either hole can end up pulling in the vortex. In about 180 kMCS, the vortex becomes pinned on one of them as seen in Fig. 5, with a net internal energy loss near $6.9J_{\rm cell}$, significantly larger than the corresponding temperature scale ($\tau = T/J_{\rm cell} = 0.0159$). The path followed by the vortex is also indicated in Fig. 5. A sense of the MC-time scale for the motion is represented in Fig. 6, which shows the distance from the dot-center to the vortex ($|\vec{X}|$) versus MC steps. After an initial relatively rapid motion (about 25 kMCS) where the vortex moves onto the line between the holes, it subsequently spends nearly 150 kMCS near the right side hole before being trapped by it. This is consistent with the shape of the potentials we estimated, which have a slight barrier surrounding the holes, which themselves have rather deep wells.

Unlike micromagnetics via the Landau Lifshitz equations, the path of the vortex is stochastic, because thermal kicks are included with the MC. Other runs with a different seed number in the Monte Carlo produce different paths, and may result in either hole pulling in the vortex. Increasing the temperature will make the path more random, however, it would take an unrealistically high temperature to get a thermal energy larger than the depth of the potential wells of the holes, even for a hole due to the removal of one magnetic atom.

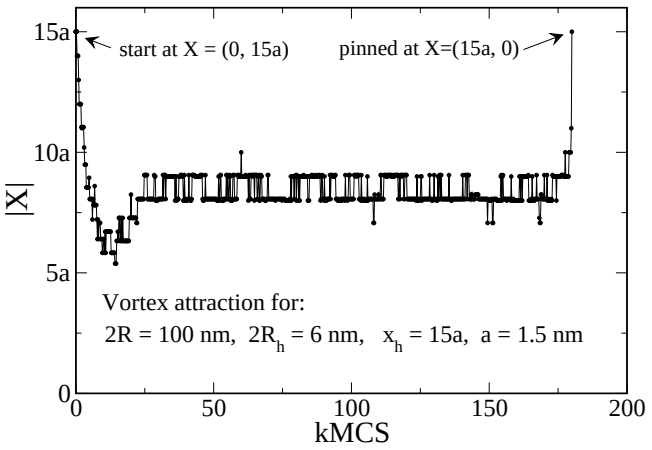

FIG. 6: The distance from the dot center to the vortex versus MC time, that results in the "vortex attraction" test by starting a vortex away from both holes as in Fig. 4.

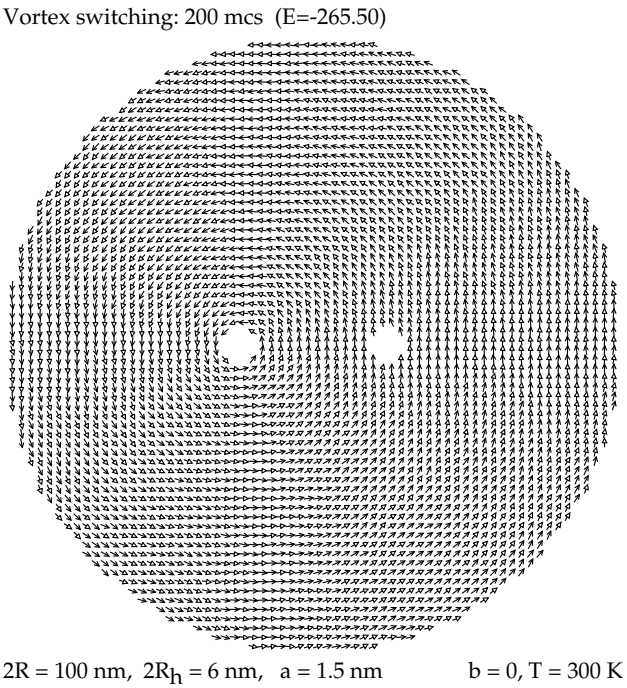

FIG. 7: Test of vortex switching between symmetric holes 12 nm from the dot center. The system diameter is 100 nm, thickness is 10 nm, and the temperature is 300 K. This is the initial relaxation state, before a magnetic field is applied.

D. Vortex switching between holes

In a more crucial set of simulations, a positive vortex is assumed to be pinned initially on one of two holes symmetrically located at $x = \pm 12$ nm, as in Fig. 7. After an initial equilibration of 2000 MCS, a uniform and constant magnetic field is applied in the direction that can tend to force a vortex out of the pinning hole towards the opposite hole. The correct field direction is perpendicular

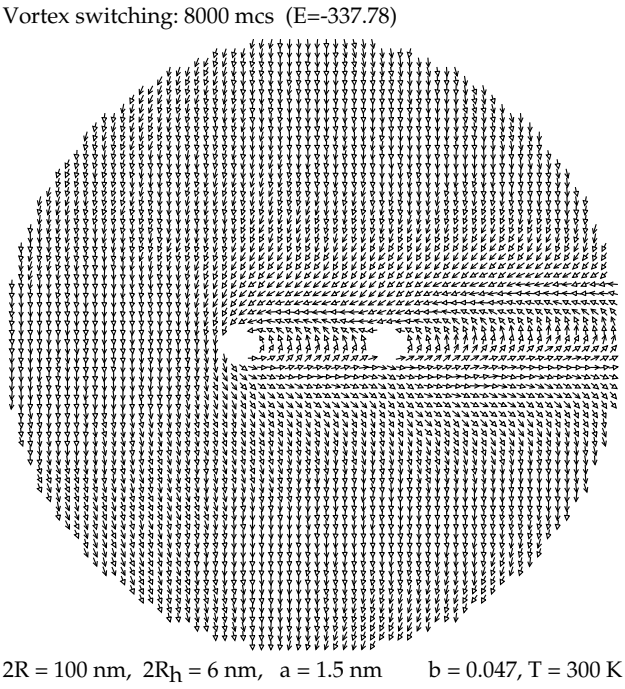

FIG. 8: Continuation of simulation in Fig. 7. After a downward magnetic field $b = 0.047$ is turned on at 2000 MCS, the spins rearrange and produce this partially polarized structure at 8000 MCS.

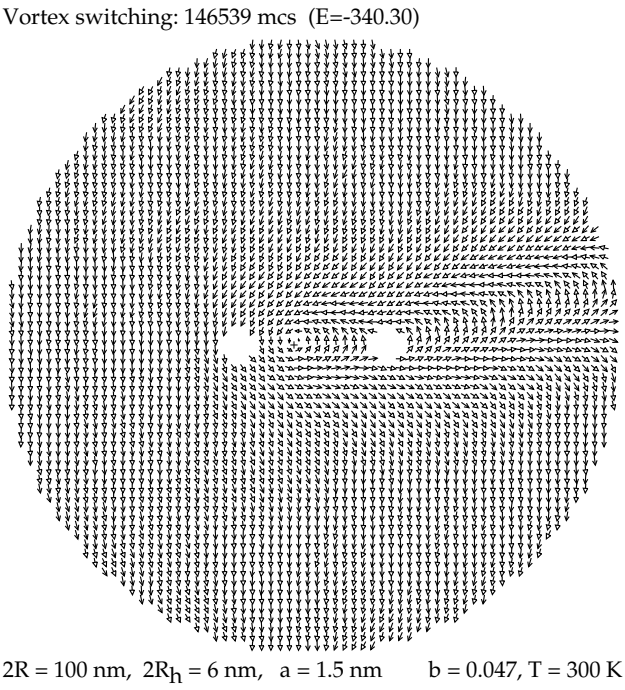

FIG. 9: Continuation of vortex switching simulation, with a downward applied magnetic field. After more than 146 kMCS the vortex emerges from the left hole and is accelerated towards the right hole. The transfer to the right hole has a duration of only 355 MCS.

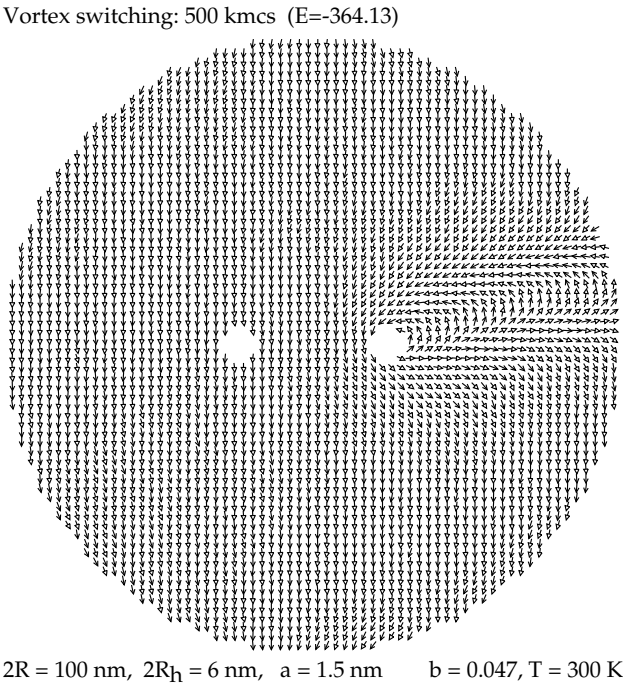

FIG. 10: End of vortex switching simulation. The vortex has become pinned on the right hole after about 147 kMCS and remains there even while the field is still turned on.

to the line connecting the holes, opposite to the dipoles between the two holes (downward in the diagrams here). That field polarizes the vortex structure, modifying it considerably, as seen in Fig. 8, which shows the situation at 8000 MCS for $b = 0.047$ or $B = 0.63$ T for Permalloy parameters. One could say that the vortex is far from "rigid." If the applied field is of adequate strength, but not excessively strong, a positive vortex emerges from the pinning hole, and is caused to move across the dot center, towards the other more energetically favorable hole, as in Fig. 9. Eventually the vortex can be affected by the effective potential of the second hole and be pulled in, resulting in a final structure as in Fig. 10.

During the vortex switching, the internal energy (not including applied magnetic field terms) changes as the vortex moves over an effective energy barrier between the holes, that is drastically diminished by the applied field. The behavior of $E_{\rm int}$ is shown in Fig. 11, for the same simulation depicted in Figs. 7–10. Consistent with the effective potentials previously estimated, the vortex must climb a very slight energy barrier upon entering the second hole. The comparison to the potentials is complicated, however, because the applied field has produced a strong polarization of the dipolar arrangement away from a perfect vortex structure that was assumed earlier. In this example, the vortex remained pinned on the second hole until the simulation was stopped at 500 kMCS.

A large enough field can de-pin the vortex from the initial hole, but if the field is excessively large, it will simply move the vortex beyond the second hole, and all

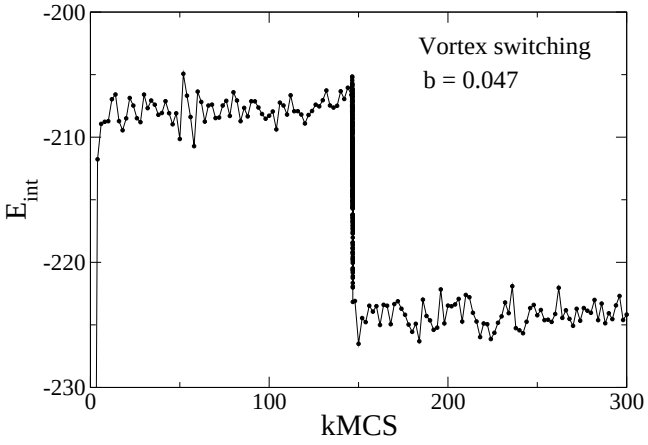

FIG. 11: For the vortex switching in Figs. 7–10, the internal energy versus Monte Carlo steps. The magnetic field turned on at 2 kMCS. Note the slight upturn in energy just before the vortex is pulled in by the second hole near 150 kMCS.

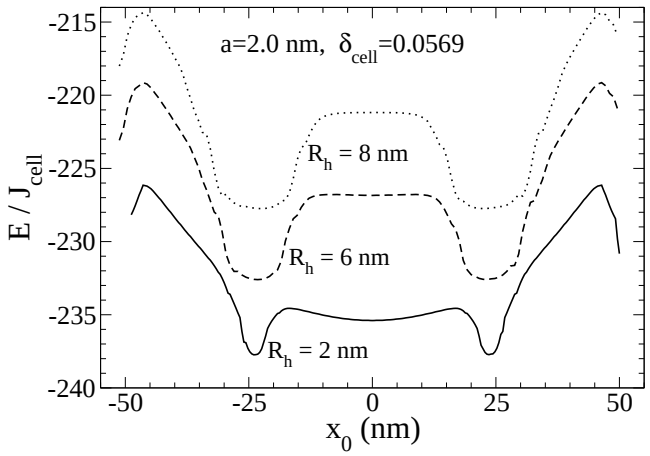

FIG. 12: For a 100 nm dot, an example of how the vortex-dot potentials depend on the size of the holes, for hole radii indicated. All the curves are on the same absolute energy scale. Larger holes raise the overall energy and tend to have deeper local wells.

the way out of the dot, as the majority of spins aligned with the field control all others. On the other hand, if the field is too small it will be unable to force the vortex out of the hole on which it is initially pinned. The critical magnetic field to initially force the vortex out of a hole, b_1, is relatively large, because it must have an equivalent energy greater than the binding energy of the vortex on the hole. For the dot parameters used (100 nm diameter, 10 nm thickness, 6 nm hole diameter), the approximate potentials indicate that the holes produce local wells with a depth of about $5J_{\rm cell}$. Considering the size of that well, it is even surprising that a dimensionless field of only $b = 0.047$ is able to free the vortex from a hole. However, after the initial relaxation out to 8000 MCS (Fig. 8), there is a strip of cells forming a domain wall between the holes, whose dipoles are not yet aligned to the applied field. It is the energy in these dipoles that must be available to free the vortex from the left hole, and that magnetic energy is of the order of the number of those cells times b, which gives about $6 \times 16 \times 0.047 J_{\rm cell} = 4.5 J_{\rm cell}$. This energy scale is similar to the depth of the well in the hole.

It is expected that the transfer onto the second hole can be made more stable for other more optimized geometries. For example, a larger diameter dot should have a deeper overall potential for containing a vortex. Also, even smaller holes have shallower potential wells; some potentials with different hole sizes are shown in Fig. 12, as found from the local dipole relaxation scheme. A smaller applied field should be able to pull a vortex out of a smaller hole, and switch it to another hole, with less danger of sweeping the vortex completely out of the dot.

Alternatively, the control of the switching could be performed by using a time-dependent applied field. A strong short burst in B might be used to initially free the vortex from its pinned position. Then once it is found between the holes, a much weaker field is needed to move it along to the opposite hole. Testing this is beyond the scope of these studies. However, the difficulty is likely to be that any sudden and strong magnetic field could produce the desired free vortex, as well as other positive or negative vortices, even ones originating from the opposite hole. Control of the entire state of the dot may be fairly complex.

V. CONCLUSIONS

The natural attraction of a vortex to a defect (or hole) is a known phenomenon, and this is a result successfully tested in the model nanomagnet with two defects present. To the extent that a vortex will get pinned on one of the holes without leaving that location, confirms the defects as more stable energetically favorable regions. Based on MC simulations, a more interesting effect should be possible: the controlled switching of a vortex from one hole to the other with the careful application of a uniform magnetic field.

An energy barrier has to be overcome to initiate the switching of the vortex from one hole to the other, primarily to pull the vortex out of the potential well of a hole. The fundamental pinning energy of the vortex within one of the holes can be attributed primarily to the removal of the core exchange energy when the vortex is pinned.

Once the vortex moves out of one of the holes as a result of the applied magnetic field, it is swept very quickly to the opposite hole by the field. The internal energy versus MC time during vortex switching demonstrates the magnitude of the net energy barrier ΔE between the holes. Without the applied field, the effective potential energy of the vortex-in-dot system has two minima for the vortex being at the hole locations. The application

of a moderate external field makes the destination hole more stable, and the initial hole less stable. This will only be true up to an upper limiting field above which the vortex will be completely swept out of the dot. With applied field between these two limiting values, the dynamics and stability of this process could be applicable to the design of bistable nanomagnetic memory devices. More study is needed to determine a more optimized geometry for stable vortex switching.

Based on the results here for a symmetrical placement of the defects, it might be possible to design more complex switching devices. For example, a pair of non-symmetrical holes should have an asymmetrical effective potential for the vortex. That arrangement could be used to to switch easily in one direction, with a more difficult switching in the opposite direction. This kind of asymmetric metastable detection device could sense one direction of magnetic field pulses above some desired threshold, while being relatively immune to the opposite field direction. Other more complex arrangements could be designed using more than two defined defects that might be able to serve as shift registers. For all of these devices based on vortex manipulation, however, the challenge may ultimately lie in the finding easy ways to discriminate the multiple states of the vortex in the dot.

Acknowledgments

This work and the visit of S. Gyan to Kansas State University were partially supported through the National Science Foundation's Research Experiences for Undergraduates program.

* Electronic address: wysin@phys.ksu.edu; URL: http://www.phys.ksu.edu/personal/wysin

† Electronic address: gyansy01@gettysburg.edu

[1] R.P. Cowburn, J. Magn. Magn. Mater. **242-245**, 505 (2002).

[2] R.P. Cowburn, D.K. Koltsov, A.O. Adeyeye, M.E. Welland and D.M. Tricker, Phys. Rev. Lett. **83**, 1042 (1999).

[3] M. Schneider, H. Hoffmann and J. Zweck, Appl. Phys. Lett. **77**, 2909 (2000).

[4] M. Hanson, O. Kazakova, P. Blomqvist, R. Wäppling and B. Nilsson, Phys. Rev. B **66**, 144419 (2002).

[5] R. Pulwey, M. Zölfl, G. Bayreuther and D. Weiss, J. Appl. Phys. **91**, 7995 (2002).

[6] M. Hehn, K. Ounadjela, J.-P. Boucher, F. Rousseaux, D. Decanini, B. Bartenlian and C. Chappert, Science **272**, 1782 (1996).

[7] O. Kazakova, M. Hanson, P. Blomqvist and R. Wäppling, J. Appl. Phys. **90**, 2440 (2001).

[8] G. Gioia and R.D. James, Proc. R. Soc. London, Ser. A **453**, 213 (1997).

[9] J.-G. Caputo, Y. Gaididei, V.P. Kravchuk, F.G. Mertens and D.D. Sheka, Phys. Rev. B **76**, 174428 (2007).

[10] N.A. Usov and S.E. Peschany, J. Magn. Magn. Mater. **118**, L290 (1993).

[11] A. Hubert and R. Schäfer, *Magnetic Domains* (springer-Verlag, Berlin, 1998).

[12] R.L. Compton and P.A. Crowell, Phys. Rev. Lett. **97**, 137202 (2006).

[13] T. Shinjo, T. Okuno, R. Hassdorf, K. Shigeto and T. Ono, Science **289**, 930 (2000).

[14] S. Hikami and T. Tsuneto, Prog. Theor. Phys. **63**, 387 (1980).

[15] S. Takeno and S. Homma, Prog. Theor. Phys. **64**, 1193 (1980); **65**, 172 (1980).

[16] M.E. Gouvêa, G.M. Wysin, A.R. Bishop and F.G. Mertens, Phys. Rev. B **39**, 11840 (1989).

[17] G.M. Wysin, M.E Gouvêa, A.R. Bishop and F.G. Mertens, in *Computer Simulation Studies in Condensed Matter Physics*, edited by D.P. Landau, K.K. Mon and H.-B. Schüttler (Springer-Verlag, Berlin, 1988).

[18] G.M. Wysin, Phys. Rev. B **49**, 8780 (1994).

[19] C.E. Zaspel and D. Godinez, J. Magn. Magn. Mater. **162**, 91 (1996).

[20] G.M. Wysin, Phys. Lett. A **240**, 95 (1998).

[21] A.R. Pereira, Phys. Lett. A **314**, 102 (2003).

[22] A.R. Pereira, L.A.S. Mól, S.A. Leonel, P.Z. Coura, and B.V. Costa, Phys. Rev. B **68**, 132409 (2003).

[23] F.M. Paula, A.R. Pereira, L.A.S. Mól, Phys. Lett. A **329**, 155 (2004).

[24] L.A.S. Mól, A.R. Pereira, and W.A. Moura-Melo, Phys. Rev. B **67**, 132403 (2003).

[25] M. Rahm, J. Biberger, V. Umansky, and D. Weiss, J. Appl. Phys. **93**, 7429 (2003).

[26] M. Rahm, R. Höllinger, V. Umansky, and D. Weiss, J. Appl. Phys. **95**, 6708 (2004).

[27] G.M. Wysin, Phys. Rev. B **68**, 184411 (2003).

[28] A.R. Pereira, J.Magn. Magn. Mater. **279**, 396 (2004).

[29] G.M. Wysin, Phys. Rev. B **71**, 094423 (2005).

[30] C.E. Zaspel, C.M. McKennan, and S.R. Snaric, Phys. Rev. B **53**, 11317 (1996).

[31] A.R. Pereira and G.M. Wysin, Phys. Rev. B **73**, 214402 (2006).

[32] A.R. Pereira, J. Appl. Phys. **97**, 094303 (2005).

[33] A.R. Pereira, Phys. Rev. B **71**, 224404 (2005).

[34] T. Uhlig, M. Rahm, C. Dietrich, R. Höllinger, M. Heumann, D. Weiss and J. Zweck, Phys. Rev. Lett. **95**, 237205 (2005).

[35] C. Kawabata, M. Takeuchi and A.R. Bishop, J. Magn. Magn. Mater. **54–57**, 871 (1986).

[36] C. Kawabata, M. Takeuchi and A.R. Bishop, J. Stat. Phys. **43**, 869 (1986).

[37] J. Sasaki and F. Matsubara, J. Phys. Soc. Japan **66**, 2138 (1997).

[38] G.M. Wysin and A.R. Bishop, Phys. Rev. B **42**, 810 (1990).

[39] M.E. Gouvêa and G.M. Wysin, Phys. Rev. B **56**, 14192 (1997).

[40] D.P. Landau, J. Magn. Magn. Mater. **200**, 231 (1999).

[41] P. Vavassori and R. Bovolenta, V. Metlushko, B. Ilic, J. Appl. Phys. **99**, 053902 (2006).

[42] G.M. Wysin, in *Electromagnetic, Magnetostatic and Exchange Interaction Vortices in Confined Magnetic Struc-*

tures, edited by Eugene Kamenetskii (Research Signpost, India 2008).
[43] K. Yu. Guslienko *et al.*, Phys. Rev. B **65**, 024414 (2002).
[44] Q.F. Xiao, J. Rudge, B.C. Choi, Y.K. Hong and G. Donohoe, Appl. Phys. Lett. **89**, 262507 (2006).
[45] J.-G. Caputo, Y. Gaididei, F.G. Mertens and D.D. Sheka, Phys. Rev. Lett. **98**, 056604 (2007).
[46] G.M. Wysin, Phys. Rev. B **54**, 15156 (1996).